Otsuka *Progress in Earth and Planetary Science* (2018) 5:57
https://doi.org/10.1186/s40645-018-0212-7

Progress in Earth and Planetary Science

REVIEW Open Access

Review of the generation mechanisms of post-midnight irregularities in the equatorial and low-latitude ionosphere

Yuichi Otsuka

Abstract

This paper provides a brief review of ionospheric irregularities that occur in magnetically equatorial and low-latitude regions post-midnight during low solar activity periods. Ionospheric irregularities can occur in equatorial plasma bubbles. Plasma bubbles are well-known to frequently occur post-sunset when the solar terminator is nearly parallel to the geomagnetic field lines (during equinoxes at the longitude where the declination of the geomagnetic field is almost equal to zero and near the December solstice at the longitude where the declination is tilted westward), especially during high solar activity conditions via the Rayleigh–Taylor instability. However, recent observations during a solar minimum period show a high occurrence rate of irregularities post-midnight around the June solstice. The mechanisms for generating the post-midnight irregularities are still unknown, but two candidates have been proposed. One candidate is the seeding of the Rayleigh–Taylor instability by atmospheric gravity waves propagating from below into the ionosphere. The other candidate is the uplift of the *F* layer by the meridional neutral winds in the thermosphere, which may be associated with midnight temperature maximums in the thermosphere.

Keywords: Equatorial ionosphere, Ionospheric irregularity, Rayleigh–Taylor instability, Plasma bubble

Introduction

Plasma bubbles, which are localized plasma density depletions in the ionosphere at equatorial and low-latitude regions, have been studied since their discovery by Booker and Wells (1938) with various radio and optical techniques (see reviews by Hysell 2000; Makela 2006; Kelley et al. 2011; Abdu 2012). Within plasma bubbles, various size scales of plasma density irregularities exist. Intense backscatter echoes caused by Bragg scattering from field-aligned irregularities (FAI) with spatial scales of one half of the radar wavelength have been observed with VHF, UHF, and L-band radars (e.g., Woodman and LaHoz 1976; Tsunoda 1980a, b). The FAI echoes are considered to be manifestations of plasma bubbles (e.g., Woodman and LaHoz 1976). Tsunoda et al. (1982) showed that FAIs observed using the ALTAIR radar were collocated with plasma depletions measured using the Atmosphere Explorer-E satellite. It is well-accepted that plasma bubbles are generated via the Rayleigh–Taylor instability that occurs at the magnetic equator after sunset when the eastward electric fields increase. In general, plasma bubbles occur frequently when the solar terminator is parallel to the geomagnetic field (during the equinoxes at the longitude where the declination of the geomagnetic field is almost equal to zero and near the December solstice at the longitude where the declination is tilted westward), and their occurrence rate increases with solar activity (Abdu et al. 1983; Tsunoda 1985; Burke et al. 2004; Nishioka et al. 2008). Such local time, seasonal, and solar activity dependences could be attributed to the magnitude of the eastward electric field at the magnetic equator. An enhancement of the eastward electric field occurs around the evening terminator in the equatorial ionosphere, known as prereversal enhancement, and increases the upward $E \times B$ drift. At the evening terminator, a thermospheric neutral wind blows eastward due to a pressure gradient toward the dayside caused by solar heating. Since the neutral wind traverses the geomagnetic field through the *F* region dynamo mechanism, upward

Correspondence: otsuka@isee.nagoya-u.ac.jp
Institute for Space-Earth Environmental Research, Nagoya University, Furo-cho, Chikusa-ku, Nagoya 464-8601, Japan

dynamo current is driven in the *F* region. Since electric current flows along the geomagnetic field, the *E* and *F* regions are coupled electro-dynamically. Due to the rapid decrease of the plasma density in the *E* region after sunset, the longitudinal gradient of the conductivity in the *E* region becomes steep at the sunset terminator. To maintain curl-free of the electric fields and/or divergence-free of the electric currents, intense eastward and westward electric fields are generated before and after the sunset terminator, respectively. Details of these mechanisms are described by Eccles et al. (2015). Prereversal enhancement is one of the most important parameters in relation to plasma bubble generation (e.g., Kelley 1989; Fejer et al. 1999).

During low solar activity conditions in recent solar cycles, however, after midnight, FAIs were frequently observed with VHF radars at magnetically low latitudes (e.g., Patra et al. 2009; Otsuka et al. 2009; Li et al. 2012; Yizengaw et al. 2013), and plasma density and electric field irregularities were observed by the C/NOFS satellite (e.g., Yokoyama et al. 2011; Dao et al. 2011; Yizengaw et al. 2013). The mechanisms generating these equatorial ionospheric irregularities are still unknown and extensively debated. The probability of plasma bubble occurrence (*P*) can be interpreted as a product of two probabilities, that is, $P = P_I \cdot P_s$, P_I is the conditional probability for the Rayleigh–Taylor instability, and P_s is the probability of seeding an instability (e.g., McClure et al. 1998). Local time, seasonal, longitudinal, and solar activity dependences for *P* are attributed to P_I. P_I could be represented in terms of the growth rate of the Rayleigh–Taylor instability. Asymmetry of the equatorial ionization anomaly between the Northern and Southern Hemispheres, which could be caused by transequatorial winds, also contributes to P_I (Maruyama and Matuura 1984). On the other hand, the day-to-day variability of *P* could be controlled by P_s because plasma bubbles occur some days but not others even in almost identical conditions for the Rayleigh–Taylor instability. Atmospheric gravity waves and plasma velocity shear at the prereversal enhancement are considered to be candidates for seeds for the Rayleigh–Taylor instability (e.g., Hysell and Kudeki 2004; Abdu et al. 2009). Atmospheric acoustic/gravity waves could be launched from severe convection in equatorial regions and propagate upward. Some of these waves could reach the ionosphere/thermosphere and seed the instability. Because the Intertropical Convergence Zone (ITCZ) is an area where tropospheric convection is active at the equatorial region (Wallset and Gautier 1993), the ITCZ can be a source of gravity waves. McClure et al. (1998) have proposed that gravity waves launched from the ITCZ could initiate the Rayleigh–Taylor instability and that the gravity wave seeding mechanisms explain the longitudinal dependence of the plasma bubble occurrence rate because the location of the ITCZ depends on the longitude and migrates northward and southward from the geographic equator mainly according to the subsolar point. However, Su et al. (2014) have reported that such a relationship between the ITCZ and plasma bubble occurrence is not clearly seen for the longitudinal dependence. During the high solar activity conditions of the equinox, P_I is high and varies day to day, so identifying the most important factors for plasma bubble generation is difficult. On the contrary, during the low solar activity conditions of the June solstice, P_I is low, so P_S may need to work effectively to generate plasma bubbles. Study of the post-midnight irregularities could elucidate plasma bubble generation mechanisms. This paper reviews recent studies of the post-midnight irregularities in equatorial and low-latitude regions and argues possible mechanisms for their generation.

Observations of post-midnight irregularities

Characteristics of occurrences

Using the Gadanki radar in India, Patra et al. (2009) have observed *F*-region FAIs post-midnight during July–August in low solar activity conditions. Figure 1 shows range-time-intensity plots of the FAI echo observed by the Gadanki radar during July 1–10, 2008. FAI echoes were detected during the post-midnight periods of those nights. Patra et al. (2009) noted that the FAI echoes were observed up to sunrise and beyond (the time of sunrise in the *F* region (300 km) is 0430 LT) and that the echo region extended to altitudes as high as 500 km on some occasions, connecting to an apex altitude of 600 km over the magnetic equator. Post-midnight FAIs were also observed by VHF radar at Hainan, China on June of 2009–2010 (Li et al. 2012). The researchers observed that the features of these FAI echoes are different from the FAIs observed post-sunset in the equinox season. In Indonesia, Otsuka et al. (2009) have carried out continuous observations of FAIs using a 30.8 MHz radar with multiple beams since February 2006. Figure 2 shows range-time-intensity (RTI) plots of the *F*-region FAI echoes observed in five beams on the night of August 21 and July 8, 2007. On the night of August 21, 2007 (Fig. 2 (right)), the FAI echoes on the beams with azimuths ranging from 180.0–125.8° lasted for more than 4 h during 2200–0400 LT with changing altitudes in the range from 200 to 350 km. Time delays between the FAI echoes of the different beams are not seen, indicating that the FAI region did not move in the zonal direction. On the other hand, on the night of July 8, 2007 (Fig. 2 (left)), FAI echoes were observed continuously during 2330–0300 LT on the easternmost beam and 0030–0500 LT on the westernmost beam. From this time delay, the trace velocity of the echo region in the zonal direction is 120 m/s westward. Using a 30.8 MHz radar in Indonesia,

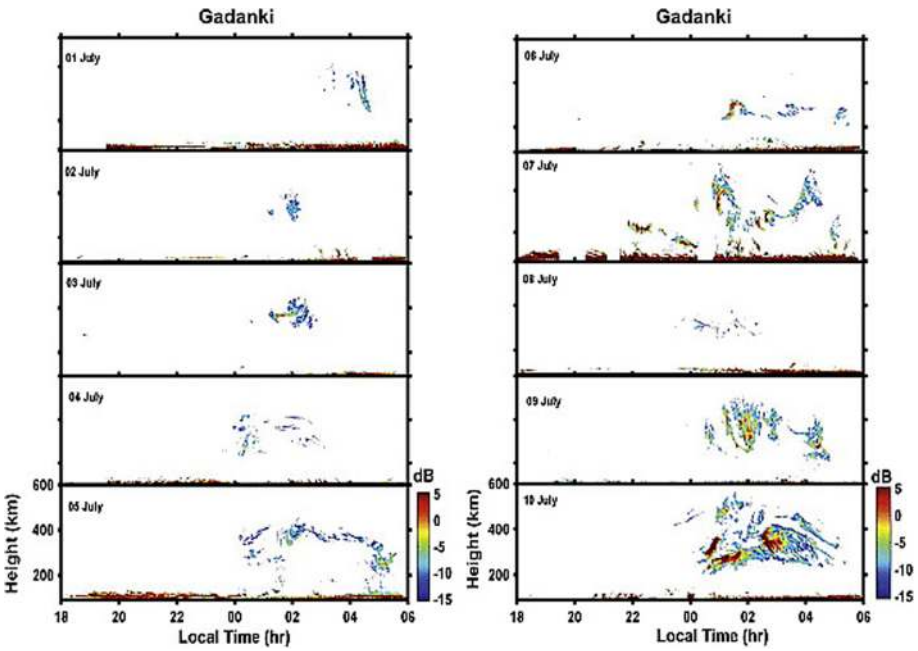

Fig. 1 Height-time variations of SNR associated with the *F*-region FAI observed by the Gadanki radar during July 1–10, 2008 (after Patra et al. 2009)

Otsuka et al. (2009, 2012) and Nishioka et al. (2012) have performed statistical studies of the FAI echo characteristics. Figure 3 shows the seasonal and local time variations of the occurrences and non-occurrences of FAI echoes from 2006 to 2010. In their study, an FAI echo was defined as an echo whose signal-to-noise ratio is larger than 0 dB and that extends more than 50 km in range. FAIs appeared most frequently post-sunset (pre-midnight) around the equinoxes and post-midnight between May and August. The yearly averages of solar flux $F_{10.7}$ were 80, 73, 68, 70, and 80 in 2006, 2007, 2008, 2009, and 2010, respectively.

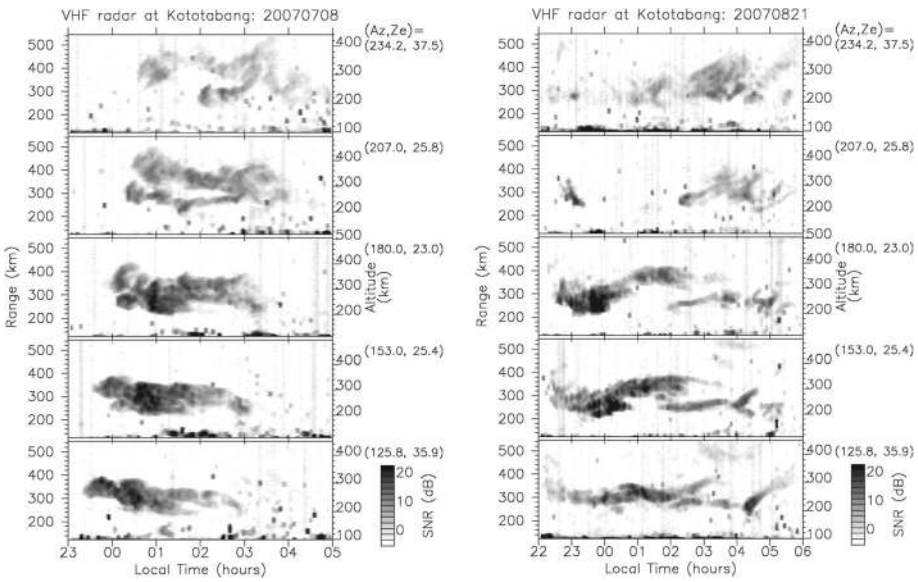

Fig. 2 Range-time-intensity plot of the FAI in the *F* region observed on the beam with azimuth of 234.2°, 207.0°, 180.0°, 153.0°, and 125.8° (from top to bottom panels) with the 30.8 MHz radar at Kototabang, Indonesia on the nights of (left) August 21, 2007, and (right) July 8, 2007. Left vertical axis shows the range from the radar and the right axis shows the altitude at which the radar beam is perpendicular to the geomagnetic field. (after Otsuka et al. 2009)

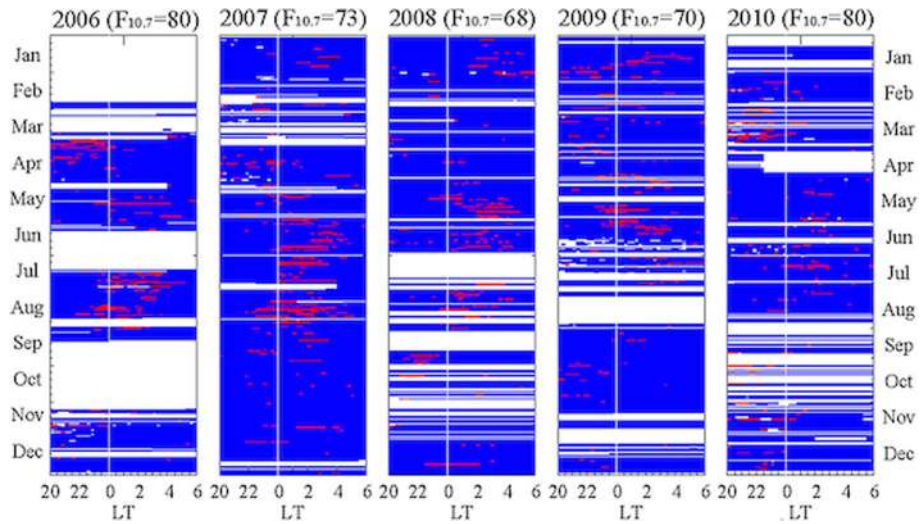

Fig. 3 Seasonal and local time variations in the *F*-region FAI echoes observed at Kototabang, Indonesia from 2006 to 2010. A signal-to-noise ratio larger than 0 dB was regarded to be an echo from an FAI. Red and blue sections represent FAI occurrences and non-occurrences, respectively, against local time and day of the year for each year from 2006 to 2010. The yearly average of the solar flux F10.7 is given at the top of each panel (after Nishioka et al. 2012)

The occurrence rates of the pre-midnight FAIs tended to increase with solar activity. On the other hand, post-midnight FAIs appeared more frequently in 2007, 2008, and 2009 than the other 2 years, indicating a negative correlation with solar activity.

By analyzing plasma density data obtained by the C/NOFS satellite, Dao et al. (2011) have reported seasonal and longitudinal variations of the plasma density irregularities occurring at magnetically equatorial and low-altitude regions in 2008 when solar activity was quite low (Fig. 4). Plasma density irregularities are found to occur frequently during May–August. This seasonal variation is consistent with the post-midnight FAIs observed with VHF radars and different from that of plasma bubbles, which frequently occur in high solar activity conditions. Furthermore, Yizengaw et al. (2013)

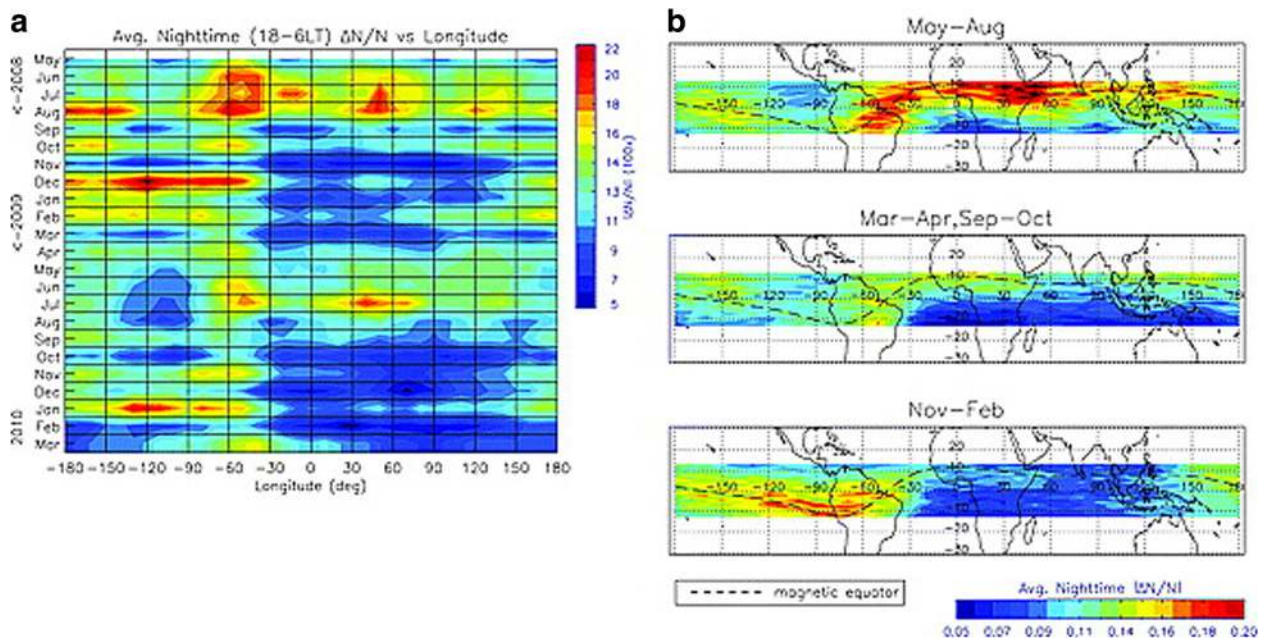

Fig. 4 **a** Average nighttime Δ*N*/*N* versus longitude over time from May 2008 to March 2010. **b** Average nighttime Δ*N*/*N* separated by seasons from observations dated May 2008 to March 2010 (after Dao et al. 2011)

have reported 4-year (2009–2012) statistics for the post-midnight irregularities observed with the C/NOFS satellite and noted that a strong occurrence peak predominantly in the African sector appears during the June solstice, indicating that the occurrence rate of post-midnight irregularities depends on the longitude.

Otsuka et al. (2012) have investigated the zonal propagation velocity of the post-midnight FAI regions by conducting five-beam measurements with the 30.8 MHz radar at Kototabang (0.20°S, 100.32°E; dip latitude 10.4°S), Indonesia and reported that 46% (14%) of the post-midnight FAIs propagated westward (eastward) and that the remaining 40% did not show discernible propagation. Figure 5 shows the local time variation of the averaged zonal propagation velocities of the post-midnight FAIs. The average propagation velocity is approximately 50 m/s westward and is invariant with time. Otsuka et al. (2012) have noted that the velocities of the post-midnight FAIs are different from that of the ambient *F*-region plasma observed with incoherent scatter radar and satellite in situ measurements (e.g., Fejer 1993; Coley and Heelis 1989). However, by analyzing the ion velocity data obtained by the C/NOFS satellite, Coley et al. (2014) have shown that the zonal plasma drift velocities largely depend on solar activity, especially pre-midnight, and that the average plasma drift velocity was westward during the midnight and post-midnight period in 2009, when solar activity was very low. Consequently, the post-midnight FAIs may mostly propagate together with the ambient plasma in the same way as the post-sunset FAIs (plasma bubbles) propagate.

Evolution of the post-midnight FAIs

By analyzing two-dimensional maps of the FAIs observed with the EAR in Indonesia, Ajith et al. (2016) have investigated the evolution of the FAI echo region within the field-of-view of the radar. They have analyzed 116 FAI events during the equinox and 45 events during the June solstice. Figure 6a, b shows the local time variation of FAI echo events during 2011–2012 for the equinox and the June solstice, respectively. During the equinoxes, 59% of the FAIs evolved between 1900 and 2000 LT and 27% during 2000–2100 LT. On the other hand, during the June solstices, 71% of FAIs evolved around midnight (2200–0300 LT), as shown in Fig. 6b.

Dao et al. (2016) have investigated the vertical rise velocities of post-midnight FAIs and found that the rise velocities of post-midnight FAIs are between 10 and 100 m/s and are smaller than those of post-sunset FAIs (from 35 to 260 m/s) (Fig. 7). Tulasi Ram et al. (2017) have calculated the rise velocity of the plasma depletion using a simulation. This velocity is consistent with those of the observed post-midnight FAIs. Based on the rise velocities, Dao et al. (2016) have estimated that the post-midnight FAIs are generated between 21:30 LT and 02:00 LT for 14 of the 15 events. These results suggest that post-midnight FAIs could be generated after the prereversal enhancement of the zonal electric fields has ceased.

Comparison with GPS scintillation

Otsuka et al. (2009) have reported seasonal and local time variations for the GPS scintillation occurrence rate in Indonesia during a solar minimum period from February 2006 to November 2007 and compared this rate to the post-midnight FAI occurrence rate (Fig. 8). While FAIs occurring after midnight were observed between May and August in 2006 and between May and September in 2007, GPS scintillation was not observed.

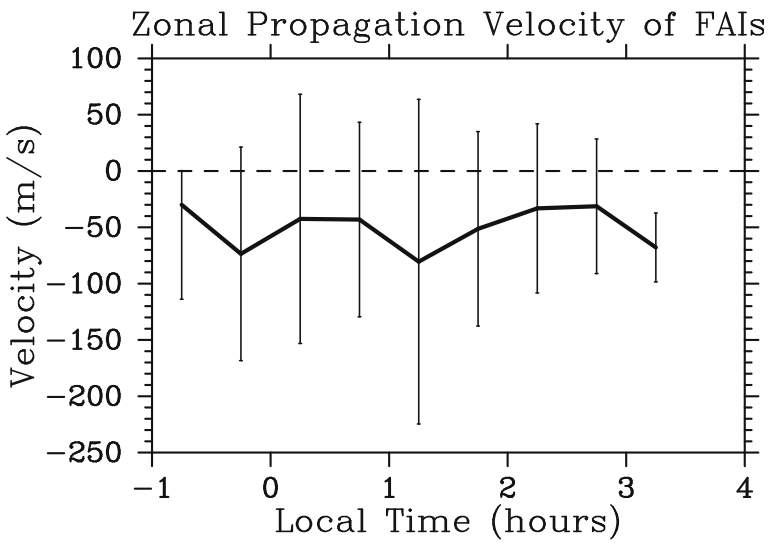

Fig. 5 Local time variation of averaged zonal propagation velocity (after Otsuka et al. 2012)

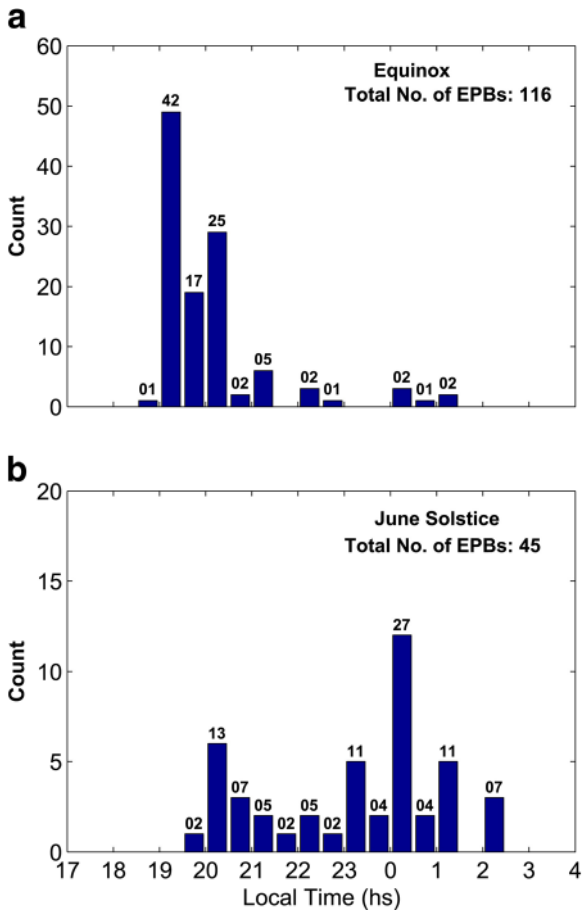

Fig. 6 Histogram showing the nighttime occurrence of freshly evolved EPBs over Kototabang during the **a** equinox and **b** June solstices from 2011 to 2012. The numbers shown on top of the histogram bars indicate percentages (after Ajith et al. 2016)

Li et al. (2012) have reported that GPS scintillation did not occur with the post-midnight FAIs observed by 47.5 MHz radar in Hainan (18.4°N, 109.6°E; dip latitude 12.8°N), China, although GPS scintillation coincided with the FAIs that occurred during the post-sunset period. Since the intensity of amplitude scintillation is proportional to the amplitude of plasma density perturbations, GPS scintillation could not be observed post-midnight during solar minimum conditions when the plasma density in the *F* region is low.

On the other hand, Akala et al. (2015) have studied the climatology of GPS amplitude scintillation over Africa from 2009 to 2011 during solar minimum and ascending conditions. Post-midnight scintillation occurred during the June solstice, although the intensity was weak. The intensity of the scintillation observed at the station near the magnetic equator was especially weaker than that observed in the crest region of the equatorial anomaly. This latitudinal variation is also interpreted from the perspective that the intensity of the amplitude scintillation is proportional to the amplitude of the plasma density perturbations. The difference between the scintillation occurrences in Asian and African regions may be related to a longitudinal dependence, as shown by satellite observations (Dao et al. 2011; Yizengaw et al. 2013). As Yizengaw et al. (2013) have shown, the post-midnight plasma irregularities in the American and African sectors extend to higher altitudes compared with those in the other longitudinal sectors. Such longitudinal differences may be responsible for why post-midnight GPS scintillation was observed in Africa but not in Asia.

Scintillation of a GPS signal is caused by plasma density perturbations at scales of 300–400 m, corresponding to the first Fresnel scale defined as $\sqrt{2\lambda z}$, where λ is the radio wavelength, and z is the altitude of the ionosphere. On the other hand, VHF radar measures meter-scale plasma density perturbations as FAI echoes. Within plasma bubbles, plasma density irregularities of various size scales are generated, but the smaller scale irregularities disappear earlier than the larger scale irregularities due to plasma diffusion (Basu et al. 1978). However, this feature is not consistent with the FAIs observed without GPS scintillation post-midnight during a solar minimum period. Sripati (2008) have suggested that the meter-scale FAIs could be generated at the gradient of kilometer-scale size irregularities as secondary instabilities and that the Rayleigh–Taylor instability that initiates a plasma bubble does not extend to the irregularities at size scales of a few hundred meters that cause GPS scintillation, resulting in an absence of GPS scintillation.

Discussion

Seeding by atmospheric gravity waves

An atmospheric gravity wave is an oscillation of neutral air that causes ion-neutral collisions and eventually generates a polarization electric field in the *F* region. Huang and Kelley (1996) have carried out numerical simulations to study the effect of gravity waves on the seeding of equatorial plasma bubbles and showed that the polarization electric fields induced by the neutral wind oscillations due to gravity waves can initiate the Rayleigh–Taylor instability and that the special resonance of the gravity waves and the plasma motion can speed up plasma bubble formation. Tsunoda (2010a) have studied the efficiency of polarization electric field generation by gravity waves in the equatorial *F* region, where the magnetic field is horizontal. Ions in the *F* region move in the $U \times B$ direction (where U is the thermospheric neutral wind and B is the magnetic field) through ion-neutral collisions and the Lorentz force, whereas electron movement is restricted to gyromotion around the magnetic field. This difference between the ion and electron

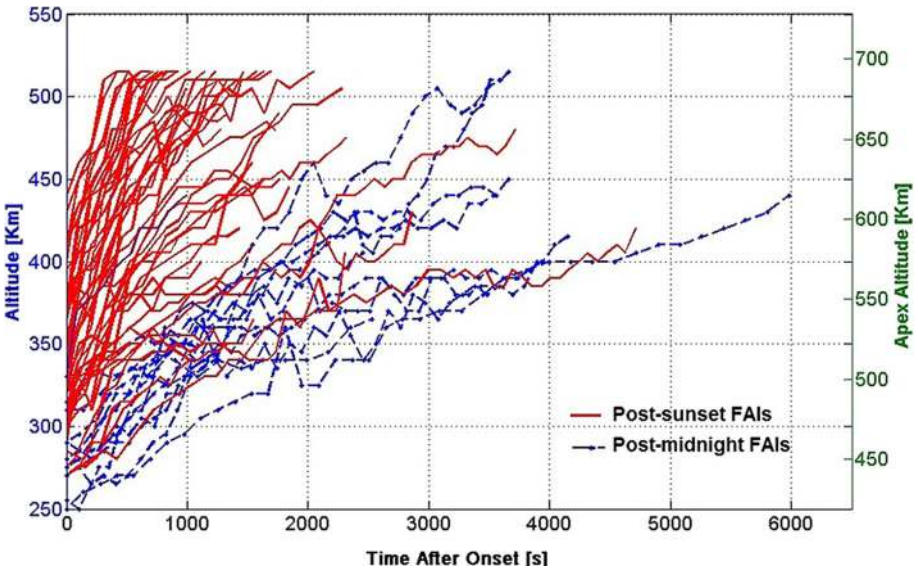

Fig. 7 Temporal variation of the top altitudes of the FAIs observed by the EAR during the growth phase. The left vertical axis shows the altitude of the location where the EAR radar beam is perpendicular to the magnetic field line. The right vertical axis shows the apex altitude of the geomagnetic field line connecting to the point measured with the EAR (after Dao et al. 2016)

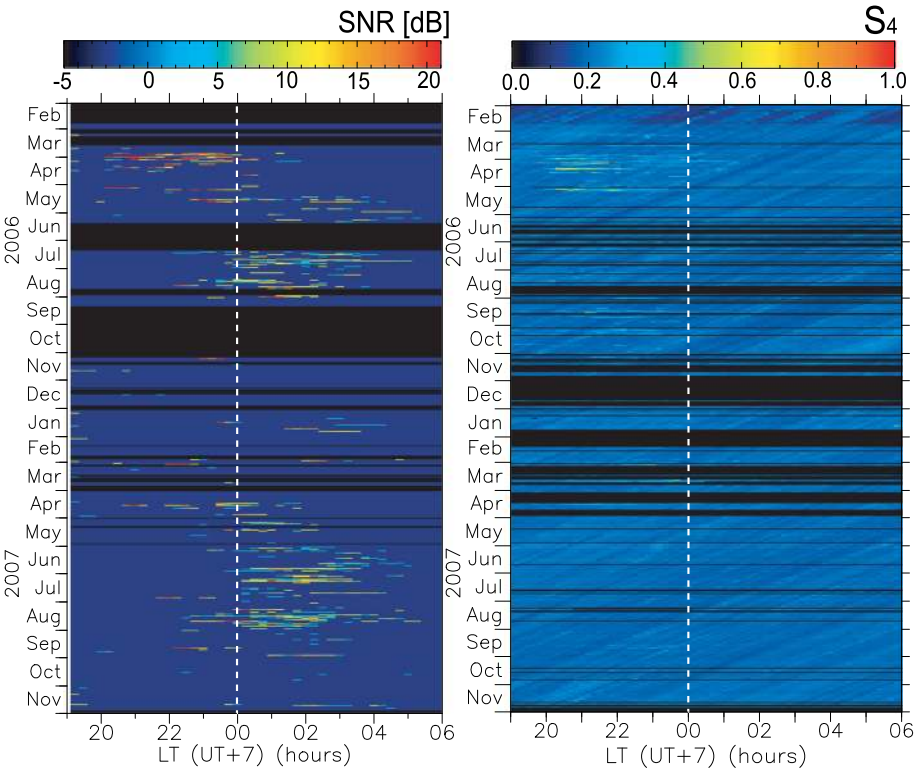

Fig. 8 Seasonal and local time variations of (left) *F*-region FAI echoes and (right) scintillation index (S4) observed at Kototabang between February 2006 and November 2007 (after Otsuka et al. 2009)

movements drives the polarization electric fields. The neutral wind oscillations due to the gravity waves in the thermosphere also drive the polarization electric fields oscillating perpendicular to the wind and magnetic fields. Tsunoda (2010a) has suggested that gravity waves with circular phase fronts effectively generate polarization electric fields through the *F* region dynamo mechanism rather than gravity waves with planar phase fronts. Figure 9 shows the configurations of the geomagnetic fields and phase fronts of the gravity waves with (a) planar and (b) circular phase fronts. As shown in Fig. 9a, when the phase front is planar, a magnetic field line pierces different phases of the gravity waves in general, except for the case where the gravity wave propagates precisely in the zonal direction when the phase front of the gravity wave is parallel to the magnetic field line. Polarization electric fields driven by the neutral wind oscillations due to gravity waves also oscillate according to the phase of the gravity wave. Since the polarization electric field can be transmitted along the magnetic field without attenuation, the electric field integrated along the magnetic field is smeared out. On the other hand, for the case of a circular phase front, the polarization electric fields are not completely smeared out because the length of the magnetic field passes through the same phase of the gravity wave depending on the radius of the circular phase front. Gravity waves with longer horizontal wavelength and monochromatic wavelength tend to have higher magnitude polarization electric fields. This researcher has also suggested that such gravity waves may produce large-scale wave structures (LSWSs). Circular patterns of plasma density perturbations in the *F* region were observed over Japan after a large earthquake (Tsugawa et al. 2011) and over the USA after a tornado (Nishioka et al. 2013) in two-dimensional maps of total electron content obtained from dense GPS receiver networks, suggesting that acoustic gravity waves can propagate from the lower atmosphere into the thermosphere with circular patterns of phase fronts. Tsunoda (2010b) has compared tropospheric convection activity with the occurrence of equatorial spread *F* (ESF), which could correspond to plasma bubbles, and found that the occurrence rate of the ESF is highest when the active convection region is located very close to the magnetic dip equator. These results indicate that atmospheric gravity waves launched from the active convection region in the troposphere could propagate into the thermosphere and contribute to plasma bubble seeding.

Seeding by medium-scale traveling ionospheric disturbances (MSTIDs)

Miller et al. (2009) have conducted simultaneous observations using an all-sky airglow imager and a VHF coherent radar and showed that after southwestward-propagating medium-scale traveling ionospheric disturbances (MSTIDs) passed through a magnetically low-latitude (close to the magnetic equator), post-midnight plasma bubbles appeared. MSTIDs, which appear frequently at mid-latitudes and propagate southeastward

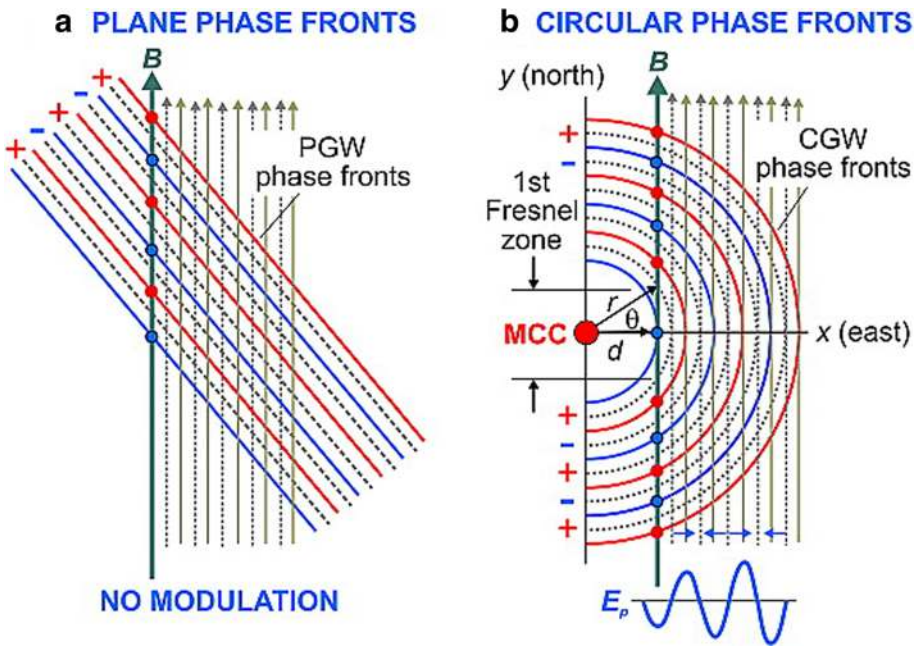

Fig. 9 Diagram showing the polarization response to the presence of gravity waves with **a** planar and **b** circular phase fronts (after Tsunoda 2010a, b)

(northwestward) in the Northern (Southern) Hemisphere, could be caused by the Perkins instability and are accompanied by polarization electric fields generated to maintain a divergence-free ionospheric current (e.g., Kelley and Makela 2000; Shiokawa et al. 2003; Otsuka et al. 2004). Miller et al. (2009) have suggested that the perturbations of the electric fields can seed the Rayleigh–Taylor instability at the magnetic equator. The seeding of plasma bubbles by MSTIDs could be a candidate for the generation of a post-midnight plasma bubble because MSTIDs accompanying electric fields occur after sunset at mid-latitudes. Candido et al. (2011) have presented seasonal and local time variations of spread *F* occurrences over Cachoeira Paulista (22.7°S, 45.0°W; MLAT 16°S), Brazil and found that the spread *F* occurrence rate is high around the June solstice (winter in the southern hemisphere) during solar minimum conditions. By carrying out simultaneous observations with an all-sky airglow imager at the same site, they have suggested that MSTIDs are one of the main sources of post-midnight irregularities. MSTIDs also can be seeded by atmospheric gravity waves (Miller et al. 1997; Kelley and Miller 1997), suggesting that atmospheric gravity waves may directly and indirectly play an important role in post-midnight irregularities.

However, such electrified MSTIDs do not always reach the magnetic equator. An equatorward boundary for the electrified MSTIDs could exist at the crest region of the equatorial anomalies (Shiokawa et al. 2002; Narayanan et al. 2014). On the other hand, at Kototabang, Indonesia, near the geographic equator, MSTIDs propagating magnetically poleward were frequently observed (Shiokawa et al. 2006; Fukushima et al. 2012). The researchers have ascertained that these poleward-propagating MSTIDs could not be accompanied by polarization electric fields. The polarization electric fields generated to maintain current continuity should be in the meridional direction because the phase front of the plasma density perturbations is elongated along the zonal direction. The electric fields in the meridional direction move ionospheric plasma only horizontally by $E \times B$ drift and thus do not form plasma density perturbations (MSTIDs). The poleward-propagating MSTIDs are assumed to be generated by atmospheric gravity waves. Further investigation is needed regarding the mechanisms of plasma bubble seeding by electrified MSTIDs.

Preferable conditions for Rayleigh–Taylor instability post-midnight

The linear growth rate (γ) of the Rayleigh–Taylor instability, which could cause an equatorial plasma bubble, is written as

$$\gamma = \left(\frac{E}{B} + \frac{g}{\nu_{\mathrm{in}}}\right)\frac{1}{n_0}\left(\frac{dn_0}{dz}\right) \quad (1)$$

where E, B, g, ν_{in}, n_0, and z are the eastward electric fie-magnetic field, gravity acceleration, ion-neutral collision frequency, plasma density in the F region, and altitude, respectively. The growth rate increases with eastward effective electric field $(\frac{E}{B} + \frac{g}{\nu_{\mathrm{in}}})$. Post-sunset, an enhancement of the eastward electric field (E), the so-called pre-reversal enhancement, plays an important role in generating a plasma bubble. During nighttime, however, the electric field is on average westward (e.g., Fejer 1991), making the growth rate negative or low. On the other hand, g/ν_{in} is larger during nighttime than daytime and increases with decreasing solar activity because ν_{in} is proportional to the neutral density, which is smaller at night than during the day and decreases with decreasing solar activity (NRLMSISE; Picone et al. 2002). The value of g/ν_{in} also increases with altitude. Therefore, the altitude of the F layer is a key parameter for plasma bubble generation. Nishioka et al. (2012) have investigated the seasonal variations of post-midnight FAI occurrence and *F*-layer altitude using an ionosonde near the magnetic equator and showed that both post-midnight FAIs and uplift of the F layer frequently occur around midnight between May and August. Figure 10 shows the seasonal and local time variations in the peak altitude of the *F*2 layer, *hmF2*, at Chumphon, Thailand, near the magnetic equator. The value for *hmF2* is calculated from *foF2* and *M(3000)F2*. This figure shows that *hmF2* enhances post-sunset (pre-midnight) around the equinoxes and post-midnight between May and August. The post-sunset enhancements are caused by prereversal enhancement of the zonal electric fields. The post-midnight enhancements coincide with the occurrences of post-midnight FAIs. Based on the observed altitude of the F layer, the researchers have evaluated the linear growth rate of the Rayleigh–Taylor instability and showed that the uplift of the F layer can enhance the growth rate due to the increase in g/ν_{in}. Figure 11a shows the seasonal variation of the *F*-layer altitude. Each cross represents *hmF2* at Chumphon at midnight, and the red curve shows the 3-month running average of *hmF2*. Since plasma bubbles are initiated at the bottom of the F layer, an altitude of 40 km below *hmF2* is assumed to be where a plasma bubble could be initiated. Figure 11b shows the seasonal variation of g/ν_{in} at a fixed altitude of 220 km (black) and at an altitude of the bottom of the F layer defined as (*hmF2*–40 km) (blue). An enhancement in g/ν_{in} at the bottom of the F layer (blue) is seen between May and August, whereas g/ν_{in} at an altitude of 220 km does not show distinct enhancement. This result indicates that the uplift of the F layer plays an important role in the growth rate. During the night, the $E \times B$ drift velocity is

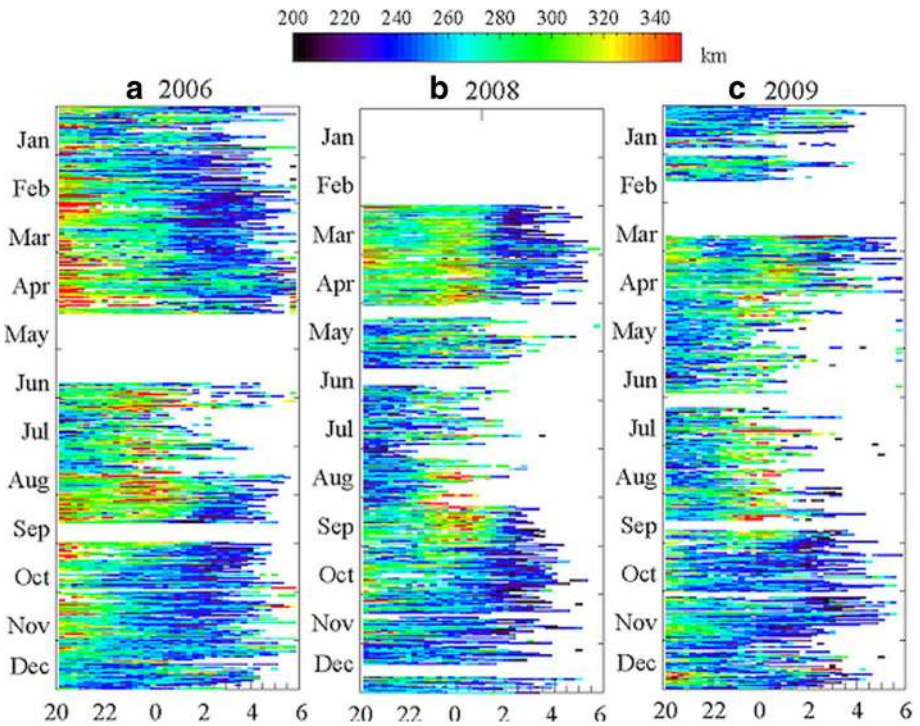

Fig. 10 Seasonal and local time variations of hmF2 at Chumphon in (**a**) 2006, (**b**) 2008, and (**c**) 2009 (after Nishioka et al. 2012)

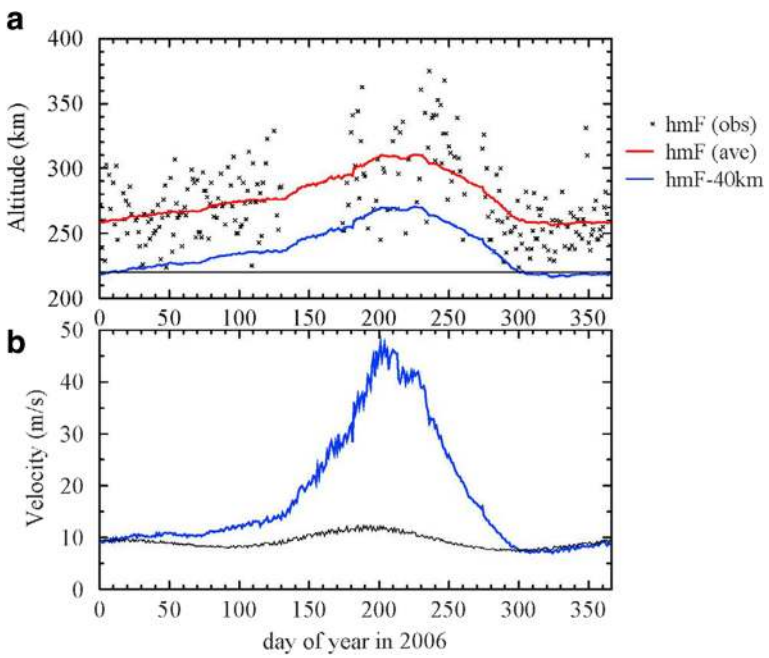

Fig. 11 (**a**) Seasonal variation of ionospheric altitude; crosses represent *hmF2* derived from *foF2* and *M(3000)F2* at Chumphon, Thailand. The running average of the daily hmF2 with a window of 3 months is shown by the red curve. The blue curve shows the altitude of the bottom-side ionosphere, which is defined as the altitude 40 km lower than the averagedhmF2 (red curve). (**b**) Estimated $g \times B$ drift velocity; the blue curve shows the $g \times B$ drift at the bottom side of the ionosphere as defined in the top panel. The black curve shows the $g \times B$ drift at a fixed altitude of 220 km (after Nishioka et al. 2012)

downward, but the seasonal average of $E \times B$ drift velocity (E/B) is approximately 10 m/s for solar minimum conditions (e.g., Fejer et al. 1991). g/ν_{in} compensates for the negative value of $E \times B$ drift velocity, and thus the growth rate or the Rayleigh–Taylor instability becomes positive. Therefore, the Rayleigh–Taylor instability may occur even near midnight through the enhanced gravity-driven eastward electric current, and plasma bubbles could grow.

Nicolls et al. (2006) have also shown observational evidence of *F*-layer uplift around midnight using an ionosonde in Brazil. Performing model calculations of the *F* layer, they have reported that the uplifts of the *F* layer around midnight are in general not caused by eastward electric fields, but a decreasing westward electric field in conjunction with sufficient recombination and plasma flux can be responsible for an uplift of the *F* layer. The weakening of the westward electric fields can be caused by an enhancement of the equatorward wind or an abatement of the poleward wind through the *F*-region dynamo mechanism. These meridional wind variations may be associated with the midnight temperature maximum (MTM). Using the SAMI2 model with $E \times B$ drift observed with the C/NOFS satellite as the input for the background electric fields, Ajith et al. (2016) have evaluated each term of the field-line-integrated growth rate and showed that a steep altitude gradient in the field-line-integrated electron content is the most important parameter for the increase of the growth rate at midnight around the June solstice. Using the SAMI3/ESF model, Huba and Krall (2013) have investigated the effect of the meridional neutral winds on the growth rate of the Rayleigh–Taylor instability. These researchers have shown that the equatorward winds at low latitudes (i.e., at a nonzero inclination of the magnetic field) could destabilize the bottom of the *F* layer by decreasing the Pedersen conductivity by the same mechanisms proposed by Maruyama et al. (2009). The parallel component of the neutral wind along the geomagnetic field carries the plasma to higher altitudes, thus reducing the Pedersen conductivity such that the bottom of the *F* layer is destabilized by the Rayleigh–Taylor instability. These researchers also observed that the eastward Pedersen current induced by the equatorward wind helps to increase the RT growth rate. Dao et al. (2017) have shown that post-midnight plasma bubbles develop toward higher altitudes/latitudes when the poleward neutral wind abated and the neutral wind became equatorward, suggesting that the equatorward neutral winds increased the growth rate of the Rayleigh–Taylor instability.

Relation to midnight temperature maximum

As described above, the uplift of the *F* layer may be a possible cause for conditions preferable for the Rayleigh–Taylor instability around midnight. However, we have a missing link; what causes the *F*-layer uplift around midnight? Nicolls et al. (2006), Yokoyama et al. (2011), and Nishioka et al. (2012) have suggested that meridional neutral winds associated with midnight temperature maximum (MTMs) can be drivers to increase the growth rate of the Rayleigh–Taylor instability by uplifting the *F* layer. MTM is a phenomenon where the neutral temperature in the thermosphere reaches a local maximum around local midnight. Niranjan et al. (2006) have suggested that MTMs more frequently occur during low solar activity conditions. This feature is consistent with the solar activity dependence of the post-midnight irregularities. Faivre et al. (2006) have shown that the amplitude of the observed neutral temperature is as high as 50–200 K. MTM could be a result of tidal phenomena and accompanied by the midnight density maximum (MDM) (Akmaev et al. 2010). The convergence of thermospheric tidal winds around the equator is considered to be responsible for generating MDMs and MTMs through adiabatic heating (Herrero 1982). Using the Thermosphere Ionosphere Electrodynamics General Circulation Model (TIEGCM), Fesen (1996) have shown that the MTM is related to atmospheric tides and that interaction of semidiurnal tides with (2, 2) and (2, 3) modes could be responsible for generating MTMs and MDMs. This researcher has further shown that these two modes reinforce each other in summer, causing frequent occurrences of MTMs in the summer hemisphere. By carrying out long-term simulations with the Whole Atmosphere Model, Akmaev et al. (2010) have revealed that the terdiurnal tide propagating upward from the lower atmosphere also plays an important role for the enhancement of the neutral temperature around midnight.

Conclusion

During solar minimum conditions, post-midnight irregularities may occur mostly in association with plasma bubbles initiated around midnight. The statistical characteristics of these post-midnight irregularities can be summarized as follows: (1) The post-midnight irregularities occur frequently around the June solstice in low solar activity conditions. Their occurrence rate increases with decreasing solar activity. (2) The regions with irregularities move mostly westward. (3) The post-midnight irregularities do not accompany GPS scintillation or weak GPS scintillation.

The mechanisms for generating these post-midnight irregularities are argued from the perspective of two aspects. The first aspect includes a seeding of the Rayleigh–Taylor instability by atmospheric gravity waves and MSTID. Gravity waves with circular phase patterns could effectively initiate the instability through the electric field perturbations caused by dynamo mechanisms. Gravity waves launched from the ITCZ may contribute to seeding the instability. MSTID associated with the

polarization electric fields may also initiate the instability. The second aspect includes *F* region conditions favorable for the Rayleigh–Taylor instability, especially the altitude of the *F* layer. The uplift of the *F* layer frequently occurs at midnight around the June solstice season and coincided with the post-midnight irregularities. The decrease in the ion-neutral collision frequency at higher altitudes increases the growth rate of the instability. The *F* layer uplift could be caused by the magnetically equatorward winds associated with MTMs.

Abbreviations

FAI: Field-aligned irregularity; MSTID: Medium-scale traveling ionospheric disturbance; MTM: Midnight temperature maximum

Acknowledgements

This work was done as a part of "Workshop on Ionospheric Plasma Bubble Seeding and Development" organized by the Institute for Space-Earth Environmental Research, Nagoya University.

Funding

This work was supported by JSPS KAKENHI Grant Number 15H05815 and 16H05736.

Availability of data and materials

Data sharing not applicable to this article as no datasets were generated or analyzed during the current study.

Author's contributions

YO wrote all the parts of the manuscript.

Author's information

YO studies the Earth's ionosphere mainly by using GNSS receivers, radar, and optical instruments.

Competing interests

The author declares that he has no competing interests.

Publisher's Note

Received: 15 November 2017 Accepted: 29 August 2018
Published online: 20 September 2018

References

Abdu MA (2012) Equatorial spread F development and quiet time variability under solar minimum conditions. Indian Journal of Radio and Space Physics 42:168–183

Abdu MA, deMedeiros RT, Bittencourt JA, Batista IS (1983) Vertical ionization drift velocities and range type spread F in the evening equatorial ionosphere. J Geophys Res 88(A1):399–402. https://doi.org/10.1029/JA088iA01p00399

Abdu MA, Kherani EA, Batista IS, de Paula ER, Fritts DC, Sobral JHA (2009) Gravity wave initiation of equatorial spread F/plasma bubble irregularities based on observational data from the SpreadFEx campaign. Ann Geophys 27:2607. https://doi.org/10.5194/angeo-27-2607-2009

Ajith KK, Tulasi Ram S, Yamamoto M, Otsuka Y, Niranjan K (2016) On the fresh development of equatorial plasma bubbles around the midnight hours of June solstice. J Geophys Res Space Physics 121. https://doi.org/10.1002/2016JA023024

Akala AO, Amaeshi LLN, Somoye EO, Idolor RO, Okoro E, Doherty PH, Groves KM, Carrano CS, Bridgwood CT, Baki P, D'ujanga FM, Seemala GK (2015) Climatology of GPS amplitude scintillations over equatorial Africa during the minimum and ascending phases of solar cycle 24. Astrophys Space Sci 357(17). https://doi.org/10.1007/s10509-015-2292-9

Akmaev RA, Wu F, Fuller-Rowell TJ, Wang H, Iredell MD (2010) Midnight density and temperature maxima, and thermospheric dynamics in whole atmosphere model simulations. J Geophys Res 115:A08326. https://doi.org/10.1029/2010JA015651

Basu S, Basu S, Aarons J, McClure JP, Cousins MD (1978) On the coexistence of kilometer- and meter-scale irregularities in the nighttime equatorial F region. J Geophys Res 83:4219–4226

Booker HG, Wells HW (1938) Scattering of radio waves by the F-region of the ionosphere. Terr Magn Atmos Electr 43(3):249–256. https://doi.org/10.1029/TE043i003p00249

Burke WJ, Huang CY, Gentile LC, Bauer L (2004) Seasonal-longitudinal variability of equatorial plasma bubble occurrence. Ann Geophys 22:3089

Candido CMN, Batista IS, Becker-Guedes F, Abdu MA, Sobral JHA, Takahashi H (2011) Spread F occurrence over a southern anomaly crest location in Brazil during June solstice of solar minimum activity. J Geophys Res 116:A06316. https://doi.org/10.1029/2010JA016374

Coley WR, Heelis RA (1989) Low-latitude zonal and vertical ion drifts seen by DE 2. J Geophys Res 94(A6):6751–6761. https://doi.org/10.1029/JA094iA06p06751

Coley WR, Stoneback RA, Heelis RA, Hairston MR (2014) Topside equatorial zonal ion velocities measured by C/NOFS during rising solar activity. Ann Geophys 32:69–75. https://doi.org/10.5194/angeo-32-69-2014

Dao E, Kelley MC, Roddy P, Retterer J, Ballenthin JO, de La Beaujardiere O, Su Y-J (2011) Longitudinal and seasonal dependence of nighttime equatorial plasma density irregularities during solar minimum detected on the C/NOFS satellite. Geophys Res Lett 38:L10104. https://doi.org/10.1029/2011GL047046

Dao T, Otsuka Y, Shiokawa K, Nishioka M, Yamamoto M, Buhari SM, Abdullah M, Husin A (2017) Coordinated observations of postmidnight irregularities and thermospheric neutral winds and temperatures at low latitudes. J Geophys Res Space Physics 122. https://doi.org/10.1002/2017JA024048

Dao T, Otsuka Y, Shiokawa K, Tulasi Ram S, Yamamoto M (2016) Altitude development of post-midnight F region field-aligned irregularities observed using Equatorial Atmosphere Radar in Indonesia. Geophys Res Lett 43:1015–1022. https://doi.org/10.1002/2015GL067432

Eccles JV, St Maurice JP, Schunk RW (2015) Mechanisms underlying the prereversal enhancement of the vertical plasma drift in the low-latitude ionosphere. J Geophys Res Space Physics 120:4950–4970. https://doi.org/10.1002/2014JA020664

Faivre M, Meriwether JW, Fesen CG, Biondi MA (2006) Climatology of the midnight temperature maximum phenomenon at Arequipa. Peru J Geophys Res 111:A06302. https://doi.org/10.1029/2005JA011321

Fejer BG (1993) F region plasma drifts over Arecibo: solar cycle, seasonal and magnetic activity effects. J Geophys Res 98(A8):13,645. https://doi.org/10.1029/93JA00953

Fejer BG, de Paula ER, Gonzalez SA, and Woodman RF (1991) Average vertical and zonal F region plasma drifts over Jicamarca. J Geophys Res, 96(A8), 13,901–13,906, doi:https://doi.org/10.1029/91JA01171

Fejer BG, Scherliess L, dePaula ER (1999) Effects of the vertical plasma drift velocity on the generation and evolution of equatorial spread F. J Geophys Res 104(A9):19859–19869. https://doi.org/10.1029/1999JA900271

Fesen CG (1996) Simulations of the low-latitude midnight temperature maximum. J Geophys Res 101(A12):26863–26874. https://doi.org/10.1029/96JA01823

Fukushima D, Shiokawa K, Otsuka Y, Ogawa T (2012) Observation of equatorial nighttime medium-scale traveling ionospheric disturbances in 630-nm airglow images over 7 years. J Geophys Res 117:A10324. https://doi.org/10.1029/2012JA017758

Herrero FA, Spencer NW (1982) On the horizontal distribution of the equatorial thermospheric midnight temperature maximum and its seasonal variation. Geophys Res Lett 9:1179–1182. https://doi.org/10.1029/GL009i010p01179

Huang CS, Kelley MC (1996) Nonlinear evolution of equatorial spread F: 1. On the role of plasma instabilities and spatial resonance associated with gravity wave seeding. J Geophys Res 101:283–292

Huba JD, Krall J (2013) Impact of meridional winds on equatorial spread F: revisited. Geophys Res Lett 40:1268–1272. https://doi.org/10.1002/grl.50292

Hysell DL (2000) An overview and synthesis of plasma irregularities in equatorial spread F. J Atmos Sol-Terr Phys 62(12):1037–1056

Hysell DL, Kudeki E (2004) Collisional shear instability in the equatorial F region ionosphere. J Geophys Res 109:A11301. https://doi.org/10.1029/2004JA010636

Kelley MC (1989) The Earth's ionosphere: plasma physics and electrodynamics. International geophysics series, vol. 43. Academic Press, New York

Kelley MC, Makela JJ, de La Beaujardière O, Retterer J (2011) Convective ionospheric storms: a review. Rev Geophys 49:RG2003. https://doi.org/10.1029/2010RG000340

Kelley MC, Makela JJ, Swartz WE, Collins SC, Thonnard S, Aponte N, Tepley CA (2000) Caribbean ionosphere campaign, year one: airglow and plasma observations during two intense midlatitude spread-F events. Geophys Res Lett 27:2825–2828

Kelley MC, Miller CA (1997) Electrodynamics of midlatitude spread F 3. Electrohydrodynamic waves? A new look at the role of electric fields in thermospheric wave dynamics. J Geophys Res 102:11,539–11,547. https://doi.org/10.1029/96JA03841
Li G, Ning B, Liu L, Wan W, Hu L, Zhao B, Patra AK (2012) Equinoctial and June solstitial *F*-region irregularities over Sanya. Indian Journal of Radio and Space Physics 42:168–183
Makela JJ (2006) A review of imaging low-latitude ionospheric irregularity processes. J Atmos Sol-Terr Phys 68(13):1441–1458
Maruyama T, Matuura N (1984) Longitudinal variability of annual changes in activity of equatorial spread *F* and plasma bubbles. J Geophys Res 89:10,903
Maruyama T, Saito S, Kawamura M, Nozaki K, Krall J, Huba JD (2009) Equinoctial asymmetry of a lowlatitude ionosphere-thermosphere system and equatorial irregularities: evidence for meridional wind control. Ann Geophys 27:2027. https://doi.org/10.5194/angeo-27-2027-2009
McClure JP, Singh S, Bamgboye DK, Johnson FS, Kil H (1998) Occurrence of equatorial *F* region irregularities: evidence for tropospheric seeding. J Geophys Res 103(A12):29119–29135. https://doi.org/10.1029/98JA02749
Miller C, Swartz W, Kelley M, Mendillo M, Nottingham D, Scali J, Reinisch B (1997) Electrodynamics of midlatitude spread F: 1. Observations of unstable, gravity wave-induced ionospheric electric fields at tropical latitudes. J Geophys Res 102:11,521–11,532. https://doi.org/10.1029/96JA03839
Miller ES, Makela JJ, Kelley MC (2009) Seeding of equatorial plasma depletions by polarization electric fields from middle latitudes:experimental evidence. Geophys Res Lett 36:L18105. https://doi.org/10.1029/2009GL039695
Narayanan VL, Shiokawa K, Otsuka Y, Saito S (2014) Airglow observations of nighttime medium-scale traveling ionospheric disturbances from Yonaguni: statistical characteristics and low-latitude limit. J Geophys Res Space Physics 119:9268–9282. https://doi.org/10.1002/2014JA020368
Nicolls MJ, Kelley MC, Vlasov MN, Sahai Y, Chau JL, Hysell DL, Fagundes PR, Becker-Guedes F, Lima WLC (2006) Observations and modeling of post-midnight uplifts near the magnetic equator. Ann Geophys 24:1317–1331
Niranjan K, Brahmanandam PS, Srivani B (2006) Signatures of equatorial midnight temperature maximum as observed from in situ and ground-based ionospheric measurements in the Indian sector. J Geophys Res 111 A07309. https://doi.org/10.1029/2005JA011386
Nishioka M, Otsuka Y, Shiokawa K, Tsugawa T, Effendy SP, Nagatsuma T, Murata KT (2012) On post-midnight field-aligned irregularities observed with a 30.8-MHz radar at a low latitude: comparison with F-layer altitude near the geomagnetic equator. J Geophys Res 117:A08337. https://doi.org/10.1029/2012JA017692
Nishioka M, Saito A, Tsugawa T (2008) Occurrence characteristics of plasma bubble derived from global groundbased GPS receiver networks. J Geophys Res 113:A05301. https://doi.org/10.1029/2007JA012605.
Nishioka M, Tsugawa T, Kubota M, Ishii M (2013) Concentric waves and short-period oscillations observed in the ionosphere after the 2013 Moore EF5 tornado. Geophys Res Lett 40:5581–5586. https://doi.org/10.1002/2013GL057963
Otsuka Y, Ogawa T, Effendy (2009) VHF radar observations of nighttime F-region field-aligned irregularities over Kototabang, Indonesia. Earth Planets Space 61(4):431–437
Otsuka Y, Shiokawa K, Nishioka M, and Effendy (2012) VHF radar observations of post-midnight F-region field-aligned irregularities over Indonesia during solar minimum, Indian J Radio Space Phys (IJRSP), 41, 199–207
Otsuka Y, Shiokawa K, Ogawa T, Wilkinson P (2004) Geomagnetic conjugate observations of medium-scale traveling ionospheric disturbances at midlatitude using all-sky airglow imagers. Geophys Res Lett 31:L15803. https://doi.org/10.1029/2004GL020262
Patra AK, Phanikumar DV, Pant TK (2009) Gadanki radar observations of F region field-aligned irregularities during June solstice of solar minimum: first results and preliminary analysis. J Geophys Res 114:A12305. https://doi.org/10.1029/2009JA014437
Picone JM, Hedin AE, Drob DP, Aikin AC (2002) NRLMSISE-00 empirical model of the atmosphere: statistical comparisons and scientific issues. J Geophys Res 107(A12):1468. https://doi.org/10.1029/2002JA009430
Shiokawa K, Otsuka Y, Ejiri MK, Sahai Y, Kadota T, Ihara C, Ogawa T, Igarashi K, Miyazaki S, Saito A (2002) Imaging observations of the equatorward limit of midlatitude traveling ionospheric disturbances. Earth Planets Space 54:57–62
Shiokawa K, Otsuka Y, Ihara C, Ogawa T, Rich FJ (2003) Ground and satellite observations of nighttime medium-scale traveling ionospheric disturbance at midlatitude. J Geophys Res. https://doi.org/10.1029/2002JA009639
Shiokawa K, Otsuka Y, Ogawa T (2006) Quasi-periodic southward-moving waves in 630-nm airglow images in the equatorial thermosphere. J Geophys Res 111:A06301. https://doi.org/10.1029/2005JA011406
Sripathi S, Bose S, Patra AK, Pant TK, Kakad B, Bhattacharyya A (2008) Simultaneous observations of ESF irregularities over Indian region using radar and GPS. Ann Geophys 26:3197–3213. https://doi.org/10.5194/angeo-26-3197-2008
Su SY, Wu CL, Kiu CH (2014) Correlation between the global occurrences of ionospheric irregularities and deep atmospheric convective clouds in the intertropical convergence zone (ITCZ). Earth Planets Space 66:134. https://doi.org/10.1186/1880-5981-66-134
Tsugawa T, Saito A, Otsuka Y, Nishioka M, Maruyama T, Kato H, Nagatsuma T, Murata KT (2011) Ionospheric disturbances detected by GPS total electron content observation after the 2011 Tohoku earthquake. Earth Planets Space 63:875–879
Tsunoda RT (1980a) Backscatter measurements of 11-cm equatorial spread-F irregularities. Geophys Res Lett 7:848
Tsunoda RT (1980b) Magnetic-field-aligned characteristics of plasma bubbles in the nighttime equatorial ionosphere. J Atmos Terr Phys 42:743–752
Tsunoda RT (1985) Control of the seasonal and longitudinal occurrence of equatorial scintillations by the longitudinal gradient in integrated E region Pedersen conductivity. J Geophys Res 90:447
Tsunoda RT (2010a) On seeding equatorial spread F: circular gravity waves. Geophys Res Lett 37:L10104. https://doi.org/10.1029/2010GL043422
Tsunoda RT (2010b) On equatorial spread F: establishing a seeding hypothesis. J Geophys Res 115:A12303. https://doi.org/10.1029/2010JA015564
Tsunoda RT, Livingston RC, McClure JP, Hanson WB (1982) Equatorial plasma bubbles: vertically elongated wedges from the bottomside F layer. J Geophys Res 87:9171–9180
Tulasi Ram S, Ajith KK, Yokoyama T, Yamamoto M, Niranjan K (2017) Vertical rise velocity of equatorial plasma bubbles estimated from Equatorial Atmosphere Radar (EAR) observations and HIRB model simulations. J Geophys Res Space Physics 122:6584–6594. https://doi.org/10.1002/2017JA024260
Wallset DE, Gautier C (1993) A satellite-derived climatology of the ITCZ. J Clim 6:2162
Woodman RF, LaHoz C (1976) Radar observations of F-region equatorial irregularities. J Geophys Res 81:5447
Yizengaw E, Retterer PEE, Roddy P, Groves K, Caton R, Baki P (2013) Post-midnight bubbles and scintillations in the quiet-time June solstice. Geophys Res Lett 40. https://doi.org/10.1002/2013GL058307
Yokoyama T, Pfaff RF, Roddy P, Yamamoto M, Otsuka Y (2011) On post-midnight low-latitude ionospheric irregularities during solar minimum: 2. C/NOFS observations and comparisons with the equatorial atmosphere radar. J Geophys Res 116:A11326. https://doi.org/10.1029/2011JA016798